Optical absorption and DFT calculations in *L*-aspartic acid anhydrous crystals: Charge carrier effective masses point to semiconducting behavior

A. M. Silva, B. P. Silva, F. A. M. Sales, and V. N. Freire
Departamento de Física, Universidade Federal do Ceará, Centro de Ciências, Caixa Postal 6030 Campus do Pici, 60455-760 Fortaleza, Ceará, Brazil

E. Moreira, U. L. Fulco, and E. L. Albuquerque
Departamento de Biofísica e Farmacologia, Universidade Federal do Rio Grande do Norte, 59072-970 Natal, Rio Grande do Norte, Brazil

F. F. Maia, Jr.
Universidade Federal Rural do Semi-Árido, Campus Angicos, 59515-000 Angicos, Rio Grande do Norte, Brazil

E. W. S. Caetano
Instituto Federal de Educação, Ciência e Tecnologia do Ceará, 60040-531 Fortaleza, Ceará, Brazil
(Received 21 May 2012; revised manuscript received 5 August 2012; published 5 November 2012)

Density functional theory (DFT) computations within the local-density approximation and generalized gradient approximation in pure form and with dispersion correction (GGA + D) were carried out to investigate the structural, electronic, and optical properties of *L*-aspartic acid anhydrous crystals. The electronic (band structure and density of states) and optical absorption properties were used to interpret the light absorption measurements we have performed in *L*-aspartic acid anhydrous crystalline powder at room temperature. We show the important role of the layered spatial disposition of *L*-aspartic acid molecules in anhydrous *L*-aspartic crystals to explain the observed electronic and optical properties. There is good agreement between the GGA + D calculated and experimental lattice parameters, with $(\Delta a, \Delta b, \Delta c)$ deviations of $(0.029, -0.023, -0.024)$ (units in Å). Mulliken [J. Chem. Phys. **23**, 1833 (1955)] and Hirshfeld [Theor. Chim. Acta **44**, 129 (1977)] population analyses were also performed to assess the degree of charge polarization in the zwitterion state of the *L*-aspartic acid molecules in the DFT converged crystal. The lowest-energy optical absorption peaks related to transitions between the top of the valence band and the bottom of the conduction band involve O $2p$ valence states and C $1p$ and O $2p$ conduction states, with the carboxyl and COOH lateral chain group contributing significantly to the energy band gap. Among the calculated band gaps, the lowest GGA + D (4.49-eV) gap is smaller than the experimental estimate of 5.02 eV, as obtained by optical absorption. Such a wide-band-gap energy together with the small carrier effective masses estimated from band curvatures allows us to suggest that an *L*-aspartic acid anhydrous crystal can behave as a wide-gap semiconductor. A comparison of effective masses among directions parallel and perpendicular to the *L*-aspartic molecules layers reveals that charge transport must be favored in the former case. Finally, we also show that there is a strong optical anisotropy in the dielectric function of *L*-aspartic acid anhydrous crystals.

DOI: 10.1103/PhysRevB.86.195201 PACS number(s): 78.55.Kz, 78.40.Me, 78.20.−e, 71.20.Rv

I. INTRODUCTION

Aspartic acid (Asp, D, and chemical formula $C_4H_7NO_4$) is one of the 20 amino acids whose polymerization gives rise to proteins. It was one of the most abundant amino acids in the primitive earth, having been found in the Murchison meteorite.[1] Asp was first discovered in 1827 by Plisson and was synthesized by boiling asparagine (which was isolated from asparagus juice in 1806) with a base.[2] As a specific cleavage site for caspases, the left-hand enantiomer *L*-aspartic acid is a key residue in apoptosis (e.g., programmed cell death) processes,[3] and after more than 30 years there is strong evidence supporting aspartate (the carboxylate anion, salt, or ester of aspartic acid) as an excitatory neurotransmitter in the central nervous system.[4]

For the gaseous aspartic acid phase, *ab initio* studies revealed a total of 139 canonical conformers, but no stable zwitterionic structure.[5] However, only 6 different conformers have been conclusively identified by their distinct rotational ^{14}N nuclear quadrupole coupling constants.[6] In solution, a total of 22 zwitterion conformers were found.[5] In the solid state, aspartic acid can be crystallized as *D* and *L* enantiomorphs at room temperature,[7] having the following crystal forms: *L*-Asp anhydrous monoclinic, $P2_1$ and $Z = 2$;[8,9] *L*-Asp monohydrated orthorhombic, $P2_12_12_1$ and $Z = 4$;[10] and *DL*-Asp anhydrous monoclinic, $C2/c$ and $Z = 8$.[11–14]

Biomolecules such as nucleotide bases, amino acids, and medicinal drugs form molecular crystals stabilized by hydrogen bonds, van der Waals interactions, and dipolar electrostatic interactions (known as salt bridges).[15] Until recently, the interest in molecular crystals remained focused mainly on the characterization of their polymorphs by infrared, Raman, nuclear magnetic resonance, and electron paramagnetic resonance spectroscopies, which are very useful in the pharmaceutical domain. On the theoretical side, the computational complexity required to study such systems within the density functional theory (DFT) approach has imposed stringent limits, as stated by Tulip and Clark.[15] As a matter of fact, even the abundant spectroscopic measurements

on molecular crystals were explained almost always by using the calculated vibrational spectra of individual biomolecules, disregarding lattice effects. However, advances in computer hardware and more efficient density functional theory codes (free and commercial) are allowing the simulation of increasingly complex systems[15] using DFT.

As our research group has pointed out in previous works,[16,17] there are efforts to employ amino acid films in biosensors and optoelectronic devices. For example, a study of the adhesion of amino acids on a series of inorganic surfaces including insulators and semiconductors was performed by Willett *et al.*,[18] while Oda and Nakayama[19,20] have proposed to control electrically the amino acid ionization and the conformation of proteins arranged on semiconductor surfaces, which might produce new types of biodevices. Stroscio and Dutta[21] described advances in synthetic nanostructures integrated with biological molecules and systems, their properties, characteristics, and functions. Thus it is of paramount importance to understand fundamental aspects (particularly, electronic and optical characteristics) of amino acid crystals and films for the future development of bio-optoelectronic devices.[17] Recently, it was demonstrated that anhydrous crystals of DNA bases are wide-gap semiconductors;[22] in the case of amino acid crystals, only a few were investigated, with results suggesting that alanine, leucine, isoleucine, and glycine[15,17] are wide-band-gap semicondutors, while valine and cysteine could be small-band-gap isolators.[15,23] The characterization of the band gap of these materials and their charge transport properties, which depend on their band structures, is relevant for the development of bio-organic electronic and optoelectronic devices[24] as well as bionanoelectronics,[25] which could advance the development of sustainable, biodegradable, biocompatible, low-cost, and mass-production electronic components.

In this work we focus on L-aspartic acid anhydrous crystals, which have a monoclinic ($P2_1$) unit cell. We have chosen this material among other amino acid crystals due to the stacking of planar L-aspartic molecules in its structure, which resembles the stacking of nucleobases in DNA molecules and in nucleobase crystals. The initial structure for the computational simulations were taken from x-ray-diffraction data,[9] its total energy being minimized using different DFT exchange-correlation functionals. The DFT optimization results also provided the electronic and optical properties of the system under study. Optical absorption measurements of L-aspartic acid anhydrous crystals in powder form were carried out, from which we have obtained an estimate for the indirect wide band gap of 5.02 eV, which is larger than the theoretical value of 4.49 eV [from the generalized gradient approximation with dispersion correction (GGA + D)]. In particular, we have given special attention to the calculation of the carrier effective masses, which is not usual, but is very important to study the charge carrier transport properties in bio-organic electronic devices. The carrier effective masses were evaluated using parabolic fittings at the band extrema and suggest that aspartic acid anhydrous crystals can have semiconductor properties like those of alanine, leucine, isoleucine, and glycine.[15,17] The values of the carrier effective masses imply that transport parallel to the molecular planes of the crystal is favored over perpendicular transport. Finally, the calculated dielectric function for polarized incident light shows a very pronounced anisotropy, much like the behavior of other amino acid crystals.

II. OPTICAL ABSORPTION MEASUREMENT

Anhydrous L-aspartic acid powder with purity greater than 99% was purchased from Sigma-Aldrich. The x-ray-diffraction measurements were accomplished to confirm the monoclinic crystal structure (data not presented here). The powder was mixed with KBr to form anhydrous L-Asp-KBr pellets. Light absorption measurements were carried out in these pellets using a Varian Cary 5000 UV-visible near-IR spectrophotometer equipped with solid sample holders. The absorption spectra of the samples were recorded in the 200–800 nm wavelength range (6.21–1.55 eV), with background removal and baseline corrections made when necessary. The onset of the optical absorption $\alpha(\hbar\omega)$ as a function of the energy in an indirect gap crystal—as our DFT calculations indicate that the anhydrous L-aspartic acid crystals have several close indirect band gaps—is related to the incident photon energy by $\alpha = C(h\nu - E_g \mp \hbar\Omega)^{1/2}$, where C is a constant, E_g is the indirect band gap, and $\mp\hbar\Omega$ is the energy of the absorbed or emitted phonon.[26,27] The square of the average optical absorption spectrum (α^2) of the anhydrous L-Asp-KBr pellets is depicted in Fig. 1. One can observe that α^2 increases gradually below 5.0 eV and sharply above this value. Accordingly, in the region where the light absorption of the anhydrous L-Asp-KBr pellets increases strongly, the indirect band gap was estimated by carrying out a linear fit of the square of the absorbance, which found a band gap energy of 5.02 eV, as shown from the straight line in Fig. 1. This value stays between the band-gap energies measured previously by our research group for monoclinic ($P2_1/n$, $Z = 4$) α-glycine crystals, 5.11 eV,[17] and for orthorhombic ($P2_12_12_1$, $Z = 4$) cysteine crystals, 4.62 eV.[23] Consequently, one can conclude from the optical absorption measurement that the anhydrous L-aspartic acid crystal is a wide-gap material.

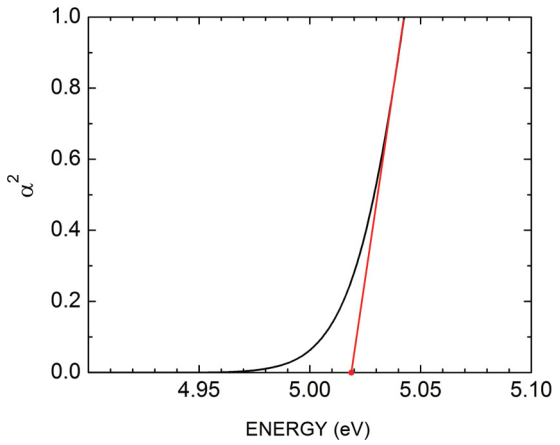

FIG. 1. (Color online) Square of the optical absorption α^2 of L-asp-KBr pellets measured at 300 K with nonpolarized incident radiation. The straight (red) line points to an estimated 5.02-eV energy gap.

III. COMPUTATIONAL DETAILS OF DFT

Quantum mechanical first-principles computations were carried out using the CASTEP code[28] to minimize the unit-cell total energy. The lattice parameters and atomic positions of anhydrous crystals of *L*-aspartic acid as measured by Derissen *et al.*[9] were used to prepare the input structure for the calculations. The x-ray data were obtained many years ago by slow evaporation of *L*-aspartic acid powder (from Fluka A. G. Buchs, high-purity degree) dissolved in an aqueous solution at room temperature.[9] It enabled the structure determination of anhydrous *L*-aspartic acid crystals and its refinement, which were found to be monoclinic with space group $P2_1$, and lattice parameters $a = 7.617$ Å, $b = 6.982$ Å, $c = 5.142$ Å, $\beta = 99.84\,^{\circ}$C, and $Z = 2$. For the sake of consistency and to improve the accuracy of experimental data, especially with respect to the hydrogen atom positioning, it is necessary to perform a DFT geometry optimization to evaluate both the unit-cell parameters and atomic coordinates. One can note, for example, that in the case of the vaterite $CaCO_3$ crystal significant differences in the spatial disposition of the carbonate groups inside the unit cell were obtained after DFT calculations in comparison with experiment.[29,30] In addition, an adequate geometry optimization is essential to calculate the vibrational properties, from which one can derive the infrared and Raman spectra whose peaks depend on the crystal geometry, amino acid side chain type, hydrogen bonding pattern, and van der Waals interactions. The same sensitivity to geometry optimization can be observed in the case of the optoelectronic properties, as when the electronic band structure varies appreciably with the lattice parameter and the atomic coordinates inside the unit cell.

The carbon backbone of the *L*-aspartic acid molecules in the crystalline phase is practically planar, the average deviation from planarity being less than 0.01 Å. Experimental values for the unit-cell parameters from Derissen *et al.*[9] are given in Table I. The *L*-aspartic acid zwitterionic molecule is depicted in Fig. 2(a), while the monoclinic unit cell of anhydrous *L*-aspartic acid crystals is shown in Fig. 2(b). Parallel layers of *L*-aspartic acid molecules can be distinguished, one being converted into the another by a screw displacement, as can be inferred from Fig. 2(c) (see also Fig. 4 in the paper of Derissen *et al.*[9]) Two adjacent layers are connected through hydrogen bonds occurring between charged groups (COO^-, NH_3^+, and COOH). Within a single layer the molecules are linked together forming zigzag chains and the chains are connected via hydrogen bonds involving the NH_3^+ group.[9] Finally, a perspective view of the existence of molecular "tunnels" in *L*-aspartic acid crystals is shown in Fig. 2(d).

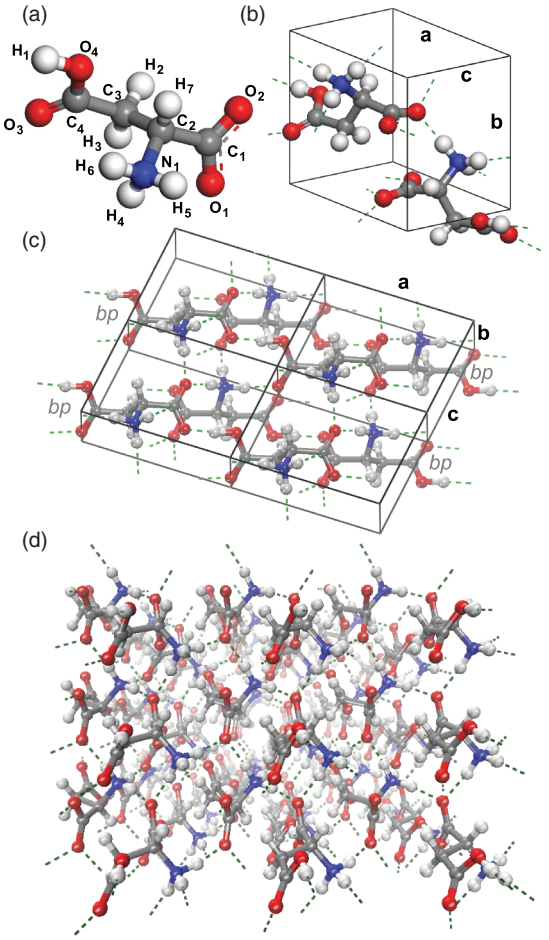

FIG. 2. (Color online) (a) The *L*-aspartic acid zwitterionic molecule; (b) the anhydrous *L*-aspartic acid monoclinic unit cell; (c) a top view of two superimposed *ab* planes of *L*-aspartic acid zwitterionic molecules, where one can be transformed into the other by a screw axis (note that the molecules in the back plane are named *bp*); and (d) perspective view of tunnels in anhydrous *L*-aspartic acid monoclinic crystals.

The DFT calculations[31,32] were carried out using the Cerpeley-Alder-Perdew-Zunger[33,34] (CAPZ) parameters for the local-density approximation (LDA) exchange-correlation functional, and the Perdew-Burke-Ernzerhof[35] (PBE) generalized gradient approximation (GGA) approach in pure form and with an extra dispersion correction scheme proposed by Tkatchenko and Scheffler.[36] The PBE functional leads to results close to the ones obtained by using the Perdew-Wang functional,[37] while dispersion correction avoids the necessity of using high-level quantum methods to describe van der

TABLE I. Lattice parameters (in Å), unit cell volume (in Å^3), and angle α (in degrees) of the anhydrous *L*-aspartic acid crystal unit cell as calculated at the LDA CAPZ and GGA PBE levels. Their deviations from experimental values (Ref. 9) are also shown.

Approximation	a (Å)	Δa (Å)	b (Å)	Δb (Å)	c (Å)	Δc (Å)	V (Å^3)	ΔV (Å^3)	β (deg)	$\Delta\beta$ (deg)
LDA	7.448	−0.169	6.712	−0.270	4.971	−0.171	243.606	−25.832	101.370	1.530
GGA	7.722	0.105	7.329	0.347	5.262	0.120	296.092	26.654	96.152	−3.688
GGA + D	7.646	0.029	6.959	−0.023	5.118	−0.024	268.880	−0.558	99.091	−0.749
Expt.	7.617		6.982		5.142		269.438		99.840	

Waals interactions. We also have adopted pseudopotentials to replace the core electrons in each atomic species. Norm-conserving pseudopotentials[38] were adopted in both the LDA and GGA + D calculations. Valence electronic configurations were used with the electronic configurations C $2s^2 2p^2$, N $2s^2 2p^3$, and O $2s^2 2p^4$. Thus each unit cell has 140 electrons (36 core and 104 valence electrons). A Monkhorst-Pack[39] $4 \times 4 \times 4$ sampling was employed to evaluate integrals in the reciprocal space. This Monkhorst-Pack grid is more than enough to give a well converged electronic structure.

Lattice parameters, angles, and atomic positions were optimized by searching a total minimum for the energy of the anhydrous *L*-aspartic acid crystals unit cell. In order to perform the geometry optimization, the following convergence thresholds were considered along successive self-consistent steps: total energy change smaller than 0.5×10^{-5} eV/atom, maximum force per atom below 0.01 eV/Å, pressure smaller than 0.02 GPa, and maximum atomic displacement below 0.5×10^{-3} Å. The Broyden-Fletcher-Goldfarb-Shanno (BFGS) minimizer[40] was employed to carry out the unit-cell optimization. In the BFGS scheme a starting Hessian is recursively updated. For each self-consistent field step, the electronic minimization parameters were a total energy/atom convergence tolerance of 0.5×10^{-6} eV, an electronic eigenenergy threshold of 0.1250×10^{-6} eV at most, and a convergence window of 3 cycles. A plane-wave basis set was adopted to represent the Kohn-Sham orbitals, with cutoff energy chosen, after convergence studies, to be 830 eV (1000 eV) in the LDA (GGA and GGA + D) computations (the cutoff energies vary due to the use of distinct pseudopotentials for each exchange-correlation functional). These energy cutoffs were good enough to ensure the absence of imaginary vibrational frequencies in our computations, indicating that well converged structures were achieved. The quality of this basis set is kept fixed as the unit-cell volume varies during geometry optimization.

After the geometry optimization, the Kohn-Sham electronic band structure and density of states (total and partial per orbital and per atom) were evaluated for both the optimized LDA and GGA + D crystals, as well as the dielectric function and optical absorption for light polarized along a set of chosen crystal directions and for a polycrystalline sample. Due to limitations of the CASTEP code, the optical properties were calculated using norm-conserved pseudopotentials only,[38] with a plane-wave energy cutoff of 800 eV. Effective masses at the extrema of the valence and conduction bands were estimated by quadratic interpolation of the corresponding band curves. The complex dielectric function $\epsilon(\omega) = \mathrm{Re}(\epsilon) + i\,\mathrm{Im}(\epsilon)$ and the optical absorption $\alpha(\omega)$ of anhydrous *L*-aspartic acid monoclinic crystals were calculated following the same scheme described in a previous work.[17]

IV. STRUCTURAL PROPERTIES

The optimized parameters of the anhydrous *L*-aspartic acid crystal unit cell, including the optimized volume V_o, are reported in Table I. Experimental values for the parameters as measured by Derissen *et al.*[9] are also shown for the sake of comparison. One can observe that the LDA calculated lattice parameters *a*, *b*, and *c* are, respectively, about −0.169, −0.270, and −0.171 Å smaller than their x-ray measured values. This volume shrinking occurs because the LDA functional tends to overestimate interatomic forces. In contrast, the calculated GGA lattice parameters are always larger than the experimental data (the pure GGA, contrary to the LDA, tends to underestimate the strength of atomic interactions), with the largest difference being observed for *b*, 0.347 Å, followed by *c*, with 0.120 Å. Indeed, of all three approaches (the LDA, GGA, and GGA + D), the pure GGA method is the least accurate in predicting the structural parameters of the anhydrous aspartic acid unit cell, notwithstanding the fact that the GGA functional provides a better description of hydrogen bonding in molecular crystals. The GGA + D approach, in comparison, has the best outcomes, with *a*, *b*, and *c*, respectively, being about 0.029 Å larger, 0.023 Å smaller, and 0.024 Å smaller than the measurements. We must then conclude that the dispersion correction is very important to compensate for the GGA underbinding in *L*-aspartic acid anhydrous crystals. The calculated unit-cell volumes are 25.832 and 0.558 $Å^3$ smaller than experiment, within the LDA and GGA + D approaches, respectively, and 26.654 $Å^3$ larger for the GGA case. In addition, the β angle is larger by 1.530° (smaller by −3.688° and −0.749°) in the LDA (GGA and GGA + D) case, in contrast with the experimental value.

The total energy variation ΔE of the anhydrous *L*-aspartic acid crystal unit cell as a function of the lattice parameter *a*, *b*, and *c* deviations relative to the optimized parameters a_o, b_o, and c_o, respectively, is shown in Fig. 3 only for the LDA and GGA + D functionals (as the GGA unit cell is the less accurate, we will not mention it in the following discussion). In order to plot the curves, we have carried out single point energy calculations for enlarged (reduced) unit cells, where the enlargement (reduction) was achieved by scaling only one of the lattice parameters of the optimized structure always, but keeping the optimized values of the fractionary atomic coordinates. As one can see, the GGA + D and LDA converged anhydrous *L*-aspartic acid crystal unit cells have the smallest total energies, as expected, and while the GGA + D functional leads to a total-energy minimum below the calculated one using the LDA framework, the total-energy curves for both functionals are very similar in shape. The total-energy dependence on Δa, Δb, and Δc is approximately

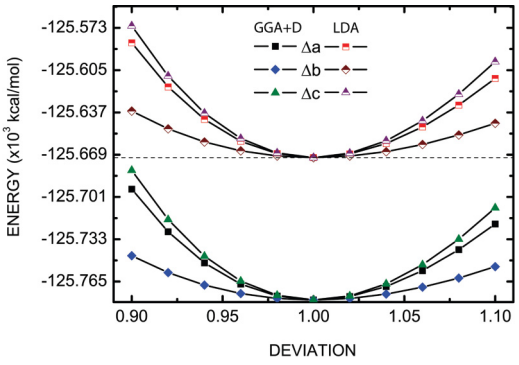

FIG. 3. (Color online) Total energy variation ΔE of the anhydrous *L*-aspartic acid crystal unit cell as a function of lattice parameter *a*, *b*, and *c* deviations relative to the optimal parameter a_o, b_o, and c_o, respectively. They were obtained at the LDA (top) and GGA + D (bottom) DFT levels of calculation.

TABLE II. Mulliken's and Hirshfeld's atomic charges of the *L*-aspartic acid molecule in the anhydrous monoclinic crystal as calculated at the LDA and GGA + D levels.

Atom	Mulliken's LDA	Mulliken's GGA	Hirshfeld's LDA	Hirshfeld's GGA
C_1	0.66	0.66	0.18	0.17
C_2	−0.16	−0.16	0.01	0.02
C_3	−0.54	−0.53	−0.10	−0.08
C_4	0.67	0.67	0.20	0.20
O_1	−0.62	−0.64	−0.17	−0.21
O_2	−0.63	−0.65	−0.18	−0.21
O_3	−0.59	−0.59	−0.18	−0.21
O_4	−0.64	−0.64	−0.14	−0.15
N_1	−0.77	−0.77	−0.10	−0.07
H_1	0.45	0.46	0.09	0.10
H_2	0.32	0.31	0.04	0.04
H_3	0.29	0.29	0.03	0.04
H_4	0.42	0.43	0.09	0.10
H_5	0.43	0.44	0.09	0.10
H_6	0.42	0.43	0.09	0.11
H_7	0.30	0.29	0.04	0.04
carboxyl	−0.59	−0.63	−0.17	−0.25
COOH lateral	−0.11	−0.10	−0.03	−0.06
amine	0.50	0.53	0.17	0.24

quadratic, with the largest concavities being observed for Δa and Δc rather than for Δb. This is due to the weaker character of the hydrogen bonds between the *L*-aspartic acid molecules at distinct molecular layers in comparison with the in plane interactions [see Fig. 2(c)].

The results of the GGA + D and LDA calculated internal atomic coordinates, bond lengths, hydrogen bond lengths, angles, and torsion angles are included in Ref. 41. The pattern of hydrogen bond distances reveals that the GGA + D functional is best suited to account for this type of bonding, so using the GGA + D instead of pure GGA and LDA exchange-correlation terms is the most accurate way to describe the main structural features of anhydrous *L*-aspartic acid crystals.

V. ELECTRONIC PROPERTIES

In Table II we present the calculated electric charges of the atoms and selected regions of the *L*-aspartic acid molecule in the anhydrous crystalline phase using two different calculation methods: Mulliken population analysis[42] (MPA) and Hirshfeld population analysis (HPA).[43] MPA is less reliable, as it arbitrarily divides the overlap electron population. For small charge transfers, Fukui function indices estimated using MPA are eventually unpredictable.[44] HPA, in contrast, is more accurate, leading to improved Fukui function indices[45,46] capable of predicting reactivity trends within a molecule better than MPA,[42] natural bond orbital analysis,[47] and fitted electrostatic potentials.[48] Moreover, HPA reduces the loss of information related to the formation of chemical bonds between atoms to form a molecule,[49,50] notwithstanding the fact that its values are systematically too small[51,52] as Hirshfeld atoms tend to resemble the neutral atoms.[53,54] This error, however, can be amended using the iterative Hirshfeld charge technique,[52] which has been successfully applied to the solid state[55] and to the discussion of Fukui functions.[56] For the charge population analysis here presented, we will focus mainly on the charges found using the HPA scheme available in the CASTEP code, followed by MPA.

The most negatively charged atoms in the *L*-aspartic acid molecule are the oxygen atoms O_1, O_2, and O_3, with Hirshfeld charges of $-0.21e$ (e is the fundamental charge, used as a unit from now on), according with the GGA + D calculations. The corresponding LDA values are $-0.17e$ (O_1) and $-0.18e$ (O_2 and O_3). The O_4 oxygen, which is bound to the C_4 and H_1 atoms, is less negative. Mulliken charge values, in contrast, are much more negative, reaching about $-0.64e$ for both exchange-correlation functionals. The most positively charged atom is the carbon atom C_1, with a Hirshfeld charge of $0.17e$ ($0.18e$) according with the GGA + D (LDA) results, which is due to the fact that C_1 is bound to two strongly negative atoms O_1 and O_2. The nitrogen atom, in contrast, has a small negative GGA + D (LDA) charge: $-0.07e$ ($-0.10e$). The carboxyl, COOH lateral chain, and amine groups have Hirshfeld GGA + D charges of $-0.25e$, $-0.06e$, and $0.24e$, respectively, which reveals the dipolar character of the zwitterionic state inside the crystal.

The Kohn-Sham electronic band structure gives a picture of the electronic eigenenergies E as a function of a set of quantum numbers that form the components of a wave vector $\mathbf{k}$ in the first Brillouin zone (BZ). For a monoclinic anhydrous *L*-aspartic acid crystal, the paths in the BZ used for the DFT computations are formed by straight segments connecting a set of high-symmetry points, as shown in Fig. 4. For the monoclinic structure, the following high-symmetry points were chosen: Γ (0,0,0), *Z* (0,0,1/2), *Y* (0,1/2,0), *A* (−1/2,1/2,0), *B* (−1/2,0,0), *C* (0,1/2,1/2), *D* (−1/2,0,1/2), and *E* (−1/2,1/2,1/2). The three primitive vectors of the reciprocal lattice $\mathbf{g}_1$, $\mathbf{g}_2$, and $\mathbf{g}_3$ are also depicted.

The GGA + D optimized electronic band structure of monoclinic anhydrous *L*-aspartic acid crystal (together with the respective partial density of states) is shown in Fig. 5.

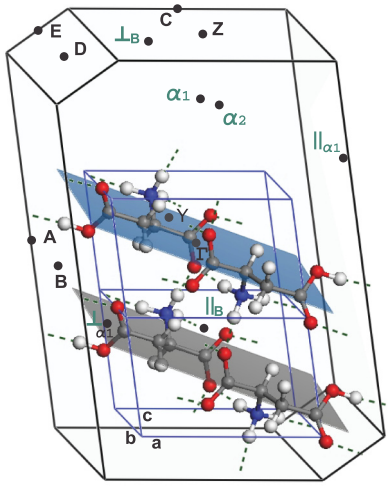

FIG. 4. (Color online) First Brillouin zone of monoclinic anhydrous *L*-aspartic acid crystals. Two planes formally distinguishing two layers of *L*-aspartic acid molecules are also depicted. High- (black letters) and low-symmetry (teal letters) points of the reciprocal lattice are indicated.

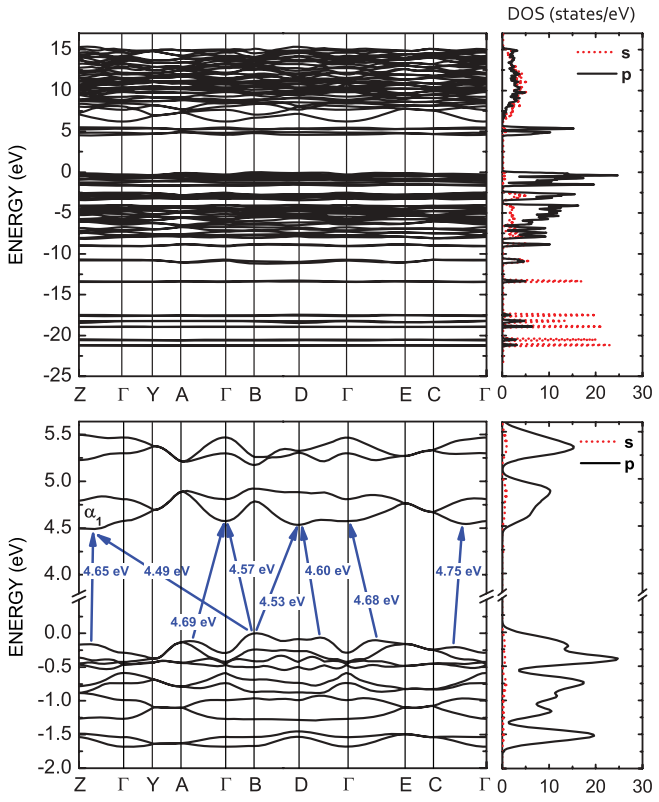

FIG. 5. (Color online) The GGA + D calculated band structure of aspartic acid anhydrous crystals (a) in the −22.5–17.5 eV range and (b) in the region around the band gap energy. The total density of states (DOS) for the orbitals *s* (dotted) and *p* (solid) are shown on the right for each case.

Energy values were gauged to ensure that the highest energy for a valence electron is equal to exactly 0 eV. At the top of Fig. 5 we have plotted the GGA + D calculated energy bands within the energy range from −22.5 to 17.5 eV. The upper valence bands are dominated by *p* states, while the deepest valence bands are mainly originated from *s* states. The bottom of the conduction band is strongly *p*-like in character, but the levels above have similar contributions from *s* and *p* states.

A closeup of the Kohn-Sham GGA + D band structure near the main band gaps of the optimized monoclinic anhydrous *L*-aspartic acid crystal is displayed in the bottom parts of Fig. 5. The LDA band structure near the main band gap (see Ref. 41) is qualitatively similar to the GGA + D one, the main differences arising from the smaller LDA values of the calculated electronic levels at the conduction bands. The smallest indirect band gap occurs between the *B* point at the valence band (VB) and the α_1 point (about one-fourth along the $Z \rightarrow \Gamma$ direction) at the conduction band (CB), which is about 4.49 eV. In comparison, the LDA smallest indirect gap energy is 4.41 eV between the *B* point at the VB and the γ_1 point at the CB (which is located between the Z-Γ line, as for α_1). All these gap values are well below the experimental gap estimate of 5.02 eV, which is expected, as pure approximated DFT functionals are not adequate to predict excitation energies.[57–61] Recently, however, a nonempirical scaling correction method for molecules and solids was proposed to correct this gap error.[62]

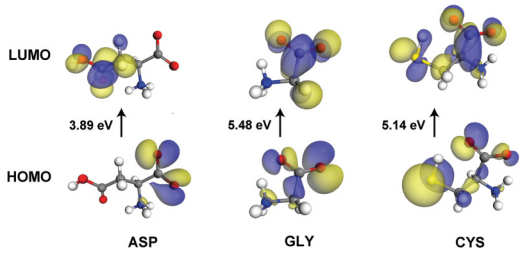

FIG. 6. (Color online) The GGA + D calculated HOMOs and LUMOs and HOMO-LUMO gaps for zwitterionic aspartic acid (left), glycine (middle), and cysteine (right) molecules. Zwitterion molecules were solvated in water to ensure stabilization.

We can compare the band-gap estimates of this work with the data previously reported in Ref. 17 for crystals of glycine and Ref. 23 for crystals of cysteine. The pure GGA main band gaps are 4.06 eV (monoclinic cysteine, CYS), 4.52 eV (orthorhombic cysteine), 4.54 eV (monoclinic aspartic acid, ASP), and 4.95 eV (monoclinic glycine, GLY), following the ordering of increasing energy values CYS < ASP < GLY. The experimental gap estimates, in contrast, are 4.62 eV (orthorhombic cysteine), 5.02 eV (monoclinic aspartic acid), and 5.11 eV (monoclinic glycine), thus obeying the same sequence CYS < ASP < GLY observed in theory, but with upward energy shifts for the monoclinic crystals of about 0.10 eV (CYS), 0.48 eV (ASP), and 0.16 eV (GLY). Aiming for a better understanding of the origin of these band gaps, we have performed DFT calculations for isolated molecules of aspartic acid, glycine, and cysteine using the GGA + D exchange-correlation functional. The molecules were kept in the zwitterionic phase by solvating the molecules in water adopting a continuous solvation scheme[63] available in the DMOL3 code.[64] After geometry optimization, we have calculated the highest occupied molecular orbital (HOMO) and the lowest unoccupied molecular orbital (LUMO). The HOMOs and LUMOs and corresponding energy gaps are shown in Fig. 6. The smallest HOMO-LUMO energy gap was calculated for aspartic acid, as 3.89 eV, while cysteine has a HOMO-LUMO gap of 5.14 eV. Glycine, by the way, has the largest energy gap value of 5.14 eV. It seems that the larger gap values observed for CYS and GLY are related to the more pronounced overlap between their HOMOs and LUMOs (especially for glycine, due to its smaller size), whereas ASP has its HOMO and LUMO states at opposite sides of the molecule, with the HOMO mostly located at the COO^- group and the LUMO mostly located at the chain side. Therefore, the HOMO-LUMO overlap is smaller and the corresponding energy gap decreases. In view of these results, returning to the crystalline phases, it seems that the larger band gap for GLY in comparison with that for ASP must be related to the pronounced intramolecular overlap of frontier electronic states in the former, while the larger band gap for ASP in comparison with CYS must be connected with the intermolecular interactions involving the planar stacking of cysteine molecules in the unit cell, which increases the orbital overlap in ASP, whereas for CYS the intermolecular interaction must effect the opposite, with the periodicity of the crystal structure contributing to a decrease of the orbital overlap and the respective band gap.

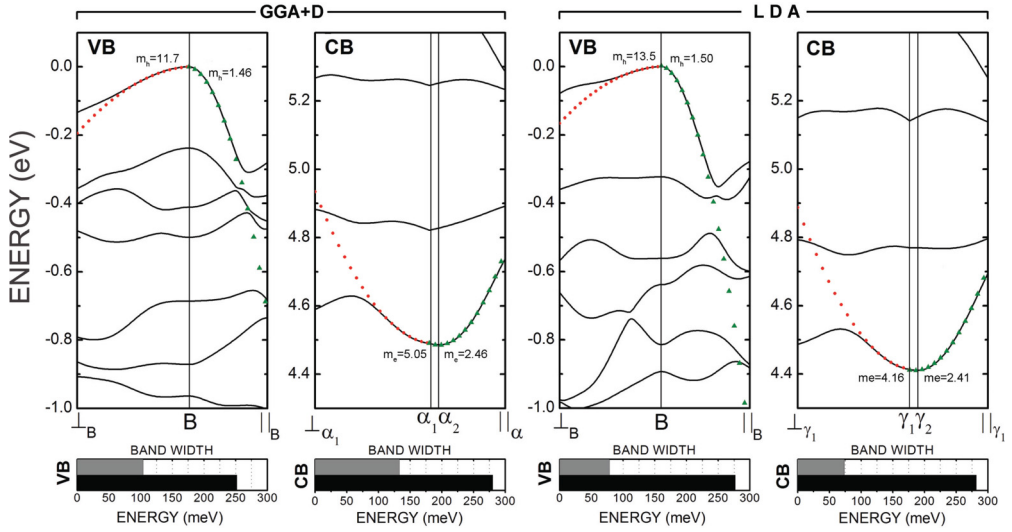

FIG. 7. (Color online) The GGA + D (left) and LDA (right) calculated valence and conduction bands along perpendicular and parallel directions to the symmetry planes formally distinguishing layers of *L*-aspartic acid molecules, as shown in Fig. 4. Values for the carrier effective mass at the band extrema are assigned, as well as the bandwidths in the perpendicular (gray bar) and parallel (black bar) directions to the symmetry axis.

We also have calculated the electronic band structures around the *B* point (which is related to the smallest indirect band gap) and around the conduction band minima. Indeed, there are two smallest energy conduction states, very close to each other, for each exchange correlation method, near the *D* point and indicated by the greek letters α_1 and α_2 in

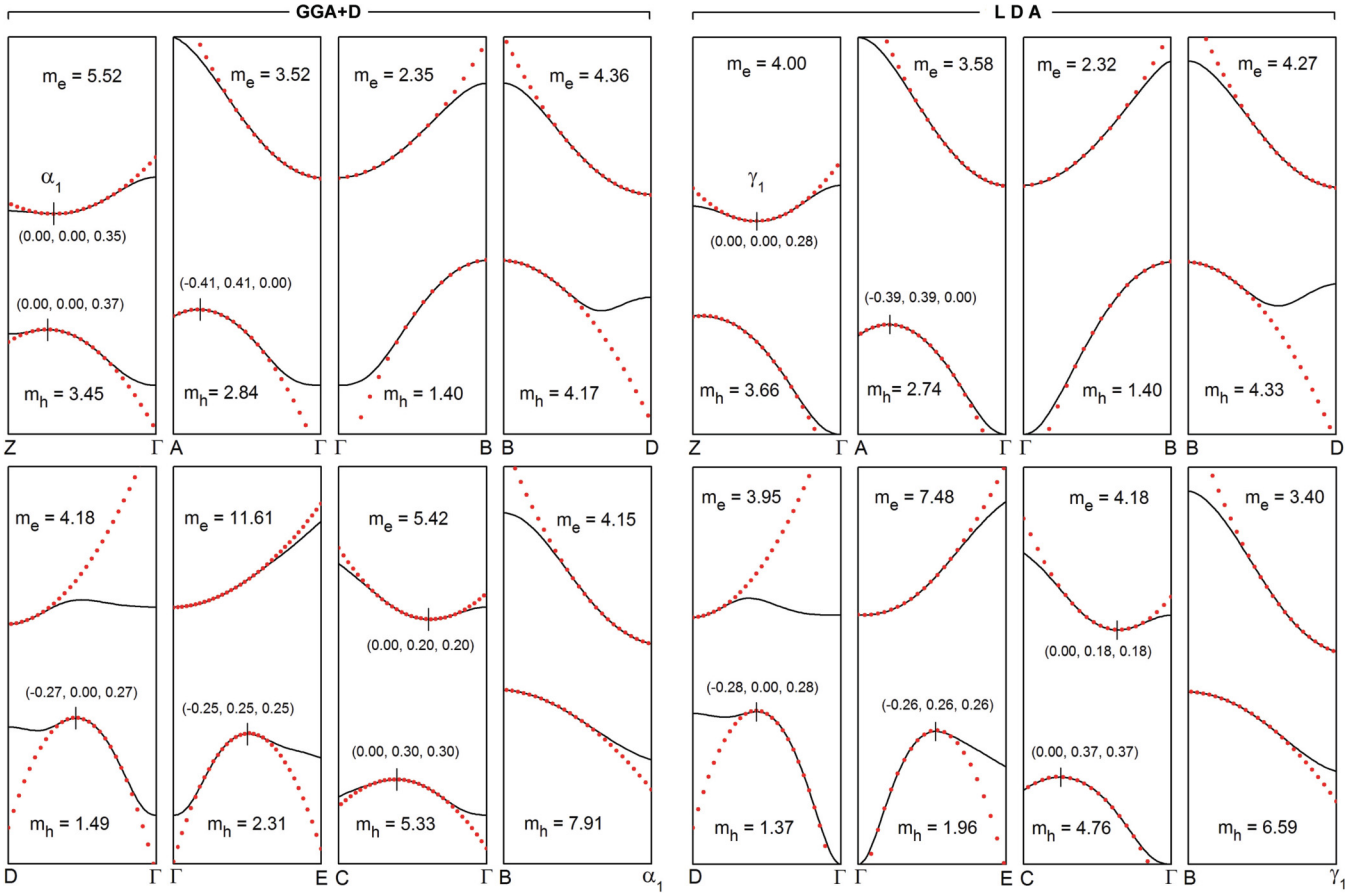

FIG. 8. (Color online) The GGA + D (left) and LDA (right) estimated electron and hole effective masses (in free-electron mass m_o unit). The fittings are performed at high- and low-symmetry points, as shown in Fig. 4.

the GGA + D case and γ_1 and γ_2 for the LDA case, along wave vectors parallel and perpendicular to the molecular layers that form the *L*-aspartic acid anhydrous crystals, as shown in Fig. 7. At the bottom we see the bandwidths for the uppermost (lowermost) valence (conduction) bands along the perpendicular (gray) and parallel (black) directions. This bandwidth is connected with the charge transport properties: Large values indicate a higher band curvature, which can be related to a lower carrier effective mass. Thus one can see that charge transport parallel to the molecular layers is easier than the perpendicular one in anhydrous crystals of *L*-aspartic acid. For example, the bandwidth for parallel holes in the GGA + D data is nearly 250 meV, while for perpendicular holes the bandwidth decreases to about 100 eV. For the conduction band, parallel electrons have a bandwidth of about 280 meV and perpendicular electrons have a bandwidth of 130 meV. The LDA figures are similar, with perpendicular hole and electron bands even thinner, having widths smaller than 80 meV.

Another way to assess the mobility of charge carriers is by calculating their effective masses. This involves a procedure wherein one calculates the band curvature at points of interest in the Brillouin zone by fitting quadratic curves. The effective mass m^* at a given point along the direction given by $\hat{\mathbf{k}}$ is

$$\frac{1}{m^*} = \frac{1}{\hbar^2}\frac{\partial^2 E(\mathbf{k} = k\hat{\mathbf{k}})}{\partial^2 k}. \quad (1)$$

Figure 7 also displays the effective masses calculated for perpendicular and parallel holes and electrons, together with the quadratic curves used to obtain their values (dots). In the GGA + D approach, the hole effective mass perpendicular to the molecular planes is almost 12 times the free-electron mass (used here as a unit), whereas within a molecular plane it decreases to only 1.46. For electrons, the perpendicular mass is 5.05 and the parallel mass is 2.46. In the LDA calculation, the calculated effective masses are nearly the same: 13.55 (1.50) for the perpendicular (parallel) hole and 4.16 (2.41) for the perpendicular (parallel) electron. We have obtained the effective masses also for other high-symmetry points and directions as well, as shown in Fig. 8. The GGA + D hole effective masses vary from 1.40 (at the *B* point along the Γ-*B* line) to 7.91 (at the *B* point along the Γ-α_1 line), whereas the electron masses vary from 2.35 (at the Γ point along the Γ-*B* line) up to 11.61 (at Γ along the Γ-*E* line). The LDA effective masses, in all cases, tend to be smaller than the corresponding GGA + D values. All in all, one can conclude that the charge carriers in *L*-aspartic acid anhydrous crystals must have very anisotropic mobilities and tend to behave as semiconductors especially if an electric field is applied along a direction parallel to the molecular planes.

In order to understand the origin of important band-structure features of monoclinic anhydrous *L*-aspartic acid crystals we must consider the relative contributions of each atomic species C, O, N, and H to the density of electronic states. They are depicted for the GGA + D calculation in the left column of Fig. 9. From them one can see that the most relevant contribution to the top of the valence band is due to O 2*p* levels, followed by a minor contribution from C 2*p* states. The bottom of the conduction band, in contrast, originates mainly from C 2*p* contributions, followed by O 2*p*. Conduction bands above 6.0 eV are dominated by H 1*s* states. The right side of Fig. 9 shows the contribution of the most important atomic groups (carboxyl, COOH lateral chain, and amine) to the electronic structure. The bottom of the valence band is mainly due to the carboxyl and COOH lateral chain groups (which could

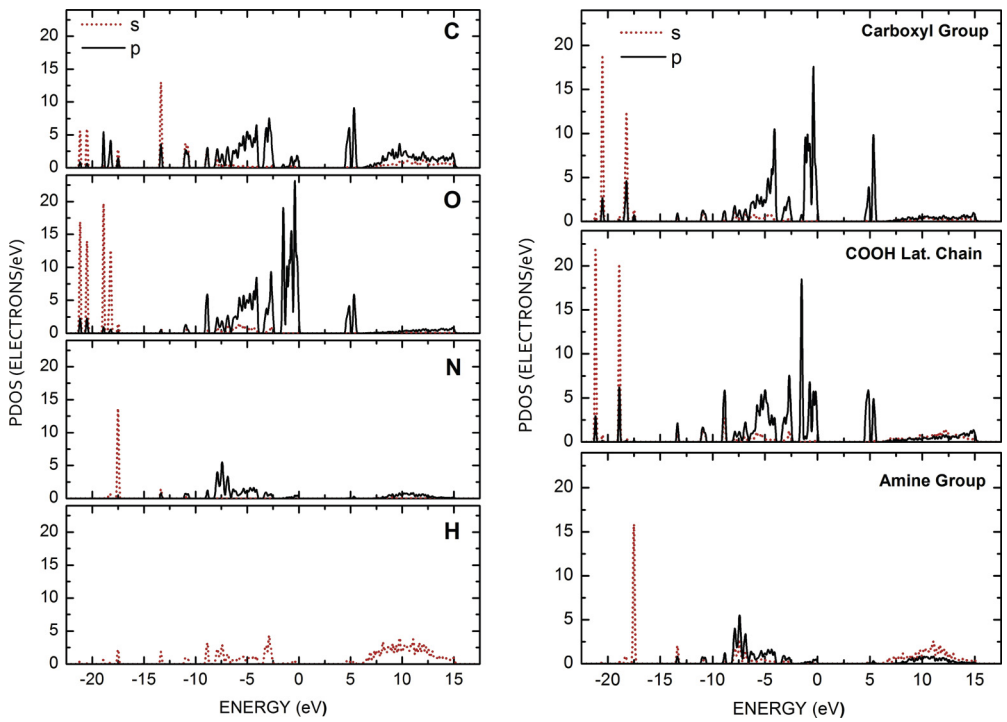

FIG. 9. (Color online) The GGA + D partial density of states (PDOS) per atom (left) and for carboxyl, the COOH lateral chain, and amine groups: *s* (dotted) and *p* (solid) orbitals.

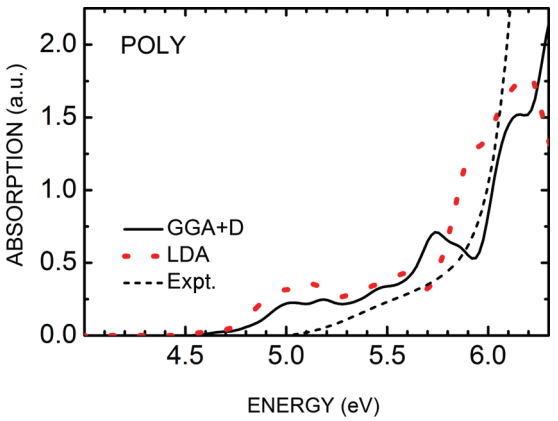

FIG. 10. (Color online) Comparison between the optical absorption of the anhydrous aspartic acid crystal measured with nonpolarized incident radiation at 300 K (dashed line) and the GGA + D (solid line) and LDA [(red) bullets] calculated (for the polycrystal).

be expected, as we have shown that O $2p$ levels dominate the electronic density of states in this region). The same occurs for the bottom of the conduction band. The main contributions of p levels related with the amine group occur between -8.0 and -4.0 eV (but smaller than the contributions of the carboxyl group and the COOH lateral chain), while above 6.0 eV, in the conduction band, amine s-like levels are the most important.

VI. OPTICAL PROPERTIES

Notwithstanding their qualitative agreement, the LDA and GGA + D approaches predict band structures with some differences in the calculated energy band gaps. For example, the smallest indirect band-gap energy obtained in the former case (4.41 eV) is 80 meV smaller than that obtained in the later case. In contrast, while reasonable agreement was obtained between the energy gap measured by optical absorption and a GGA estimate for monoclinic α glycine ($E_{\text{expt}} = 5.11$ eV and $E_{[Z,\Gamma]\to\Gamma} = 4.95$ eV),[17] as well as for orthorhombic cysteine crystals ($E_{\text{expt}} = 4.62$ eV and $E_{\Gamma\to Z} = 4.52$ eV),[23] the GGA + D estimated indirect energy gap $E_{B-\alpha_{1,\text{GGA+D}}} = 4.49$ eV for monoclinic anhydrous L-aspartic acid crystals is considerably smaller than the energy gap measured by optical absorption $E_{\text{expt}} = 5.02$ eV, as already depicted in Fig. 1. Looking now to Fig. 10, we can perform a direct comparison between the optical absorption measurements and the calculated optical absorption from the LDA and GGA + D computations in this work, for the case of a polycrystalline sample. One can see that both theoretical curves have their onsets above 4.7 eV, very close to the smallest calculated direct band gaps. The GGA + D absorption curve exhibits peaks at about 5.0, 5.2, 5.4, 5.7, 5.8, and 6.1 eV, whereas the LDA curve has peaks at about 5.0, 5.2, 5.6, 5.9, and 6.1 eV. One can note that both the GGA + D and LDA results behave similarly for energies up to 5.6 eV, with some qualitative differences being noticeable for energies between 5.6 and 6.3 eV. The experimental absorption onset, in contrast, does not exhibit

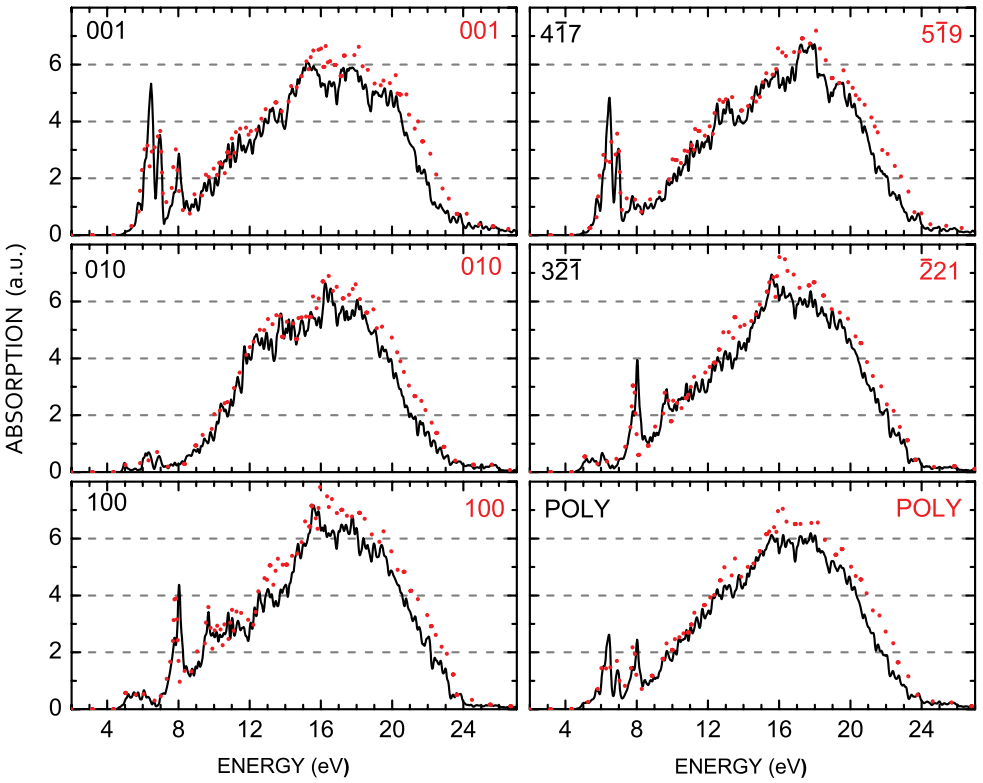

FIG. 11. (Color online) The GGA + D (solid line) and LDA (dotted line) calculated optical absorption of the anhydrous aspartic acid crystal along the directions 001, 010, 100, 4$\bar{1}$7, and 3$\bar{2}\bar{1}$ for the former and 001, 010, 100, 5$\bar{1}$9, and $\bar{2}$21 for the latter. The optical absorption for the polycrystal is also shown.

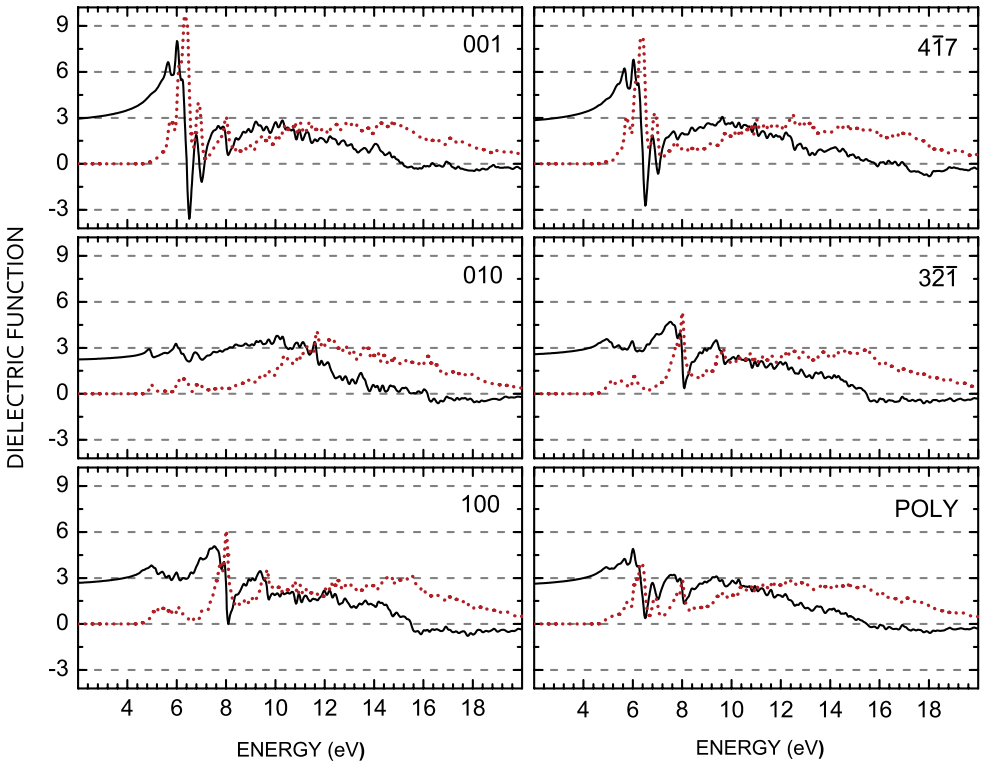

FIG. 12. (Color online) Real (solid line) and imaginary (dotted line) components of the GGA + D calculated dielectric function of the anhydrous aspartic acid crystal along the directions 001, 010, 100, 4$\bar{1}$7, and 3$\bar{2}\bar{1}$. The dielectric function components for the polycrystal are also shown.

any peak structure in the range of energies investigated, but increases sharply at about 6.0 eV.

Figure 11 depicts the optical absorption obtained from the LDA and GGA + D electronic structures in the case of incident light polarized along some selected planes of the crystal. From them one can see that *L*-aspartic acid crystals are remarkably anisotropic for light absorption, mainly for photon energies below 10 eV, independently from the chosen exchange-correlation functional. For example, the GGA + D absorption spectrum for light polarized along the 001 crystalline plane has a series of well defined absorption peaks between 6.0 and 7.0 eV, which are very attenuated or absent for light with 010 and 100 polarizations. The absorption spectrum for the directions 4$\bar{1}$7 and 3$\bar{2}\bar{1}$, which correspond to the directions parallel and perpendicular to the molecular planes of *L*-aspartic acid, are very similar, respectively, to the 001 and 100 curves, for energies up to 10 eV. In the LDA case, these directions are 5$\bar{1}$9 (parallel) and $\bar{2}$21 (perpendicular).

Finally, Figs. 12 and 13 show the real and imaginary parts of the dielectric function $\epsilon(\omega) = \epsilon_1(\omega) + i\epsilon_2(\omega)$ calculated using the GGA + D and LDA exchange-correlation functionals, in this order. The imaginary part ϵ_2 is proportional to the optical absorption we have discussed in the preceding paragraph, so we focus now on the analysis of the real part ϵ_1. For the 001 direction, $\epsilon_1(\omega = 2.0\ \text{eV})$ is approximately 3.0 (3.2) using the GGA + D (LDA) functional, whereas for a photon energy of 20.0 eV, ϵ_1 is slightly negative (negative). Maximum values of ϵ_1 for the GGA + D curve occur near 6.0 eV and between 7.0 and 14 eV, while a minimum value of ϵ_1 below -3.0 occurs for a photon energy of 6.5 eV (7.0 eV in the LDA case). Along the 010 and 100 directions, the GGA + D (LDA) values for $\epsilon_1(\omega = 2.0\ \text{eV})$ are 2.2 and 2.8 (2.4 and 2.9), respectively, with the 010 polarization exhibiting a small variation for energies between 2.0 and 11.5 eV, decreasing to approximately zero between 12.5 and 16.0 eV. The 100 polarization, iin contrast, has ϵ_1 maxima at 4.8, 7.5, and 9.3 eV and a minimum $\epsilon_1 \approx 0$ for a photon energy of 8.1 eV. As noted for the optical absorption, ϵ_1 along the directions parallel and perpendicular to the *L*-aspartic acid molecular planes is very similar to the 001 and 100 curves for both GGA + D and LDA results. The polycrystalline case, in contrast, shares many features with the 001 direction in the energy range between 2.0 and 8.0 eV.

VII. CONCLUSION

We have performed density functional calculations to obtain optimized geometries and optoelectronic properties of *L*-aspartic acid anhydrous crystals. We also have presented the experimental absorption spectrum of the anhydrous *L*-aspartic acid powder, inferring an indirect band gap of about 5.02 eV, which is smaller (larger) than previous measurements for glycine (cysteine) crystals. The LDA, GGA, and GGA + D exchange-correlation functionals were employed to optimize the geometry of the crystal unit cell, with the GGA + D results in excellent agreement with available x-ray-diffraction data (an error of only 0.558 Å^3, or -0.21%, relative to the experimental unit-cell volume) and the GGA structural parameters displaying the largest differences in comparison

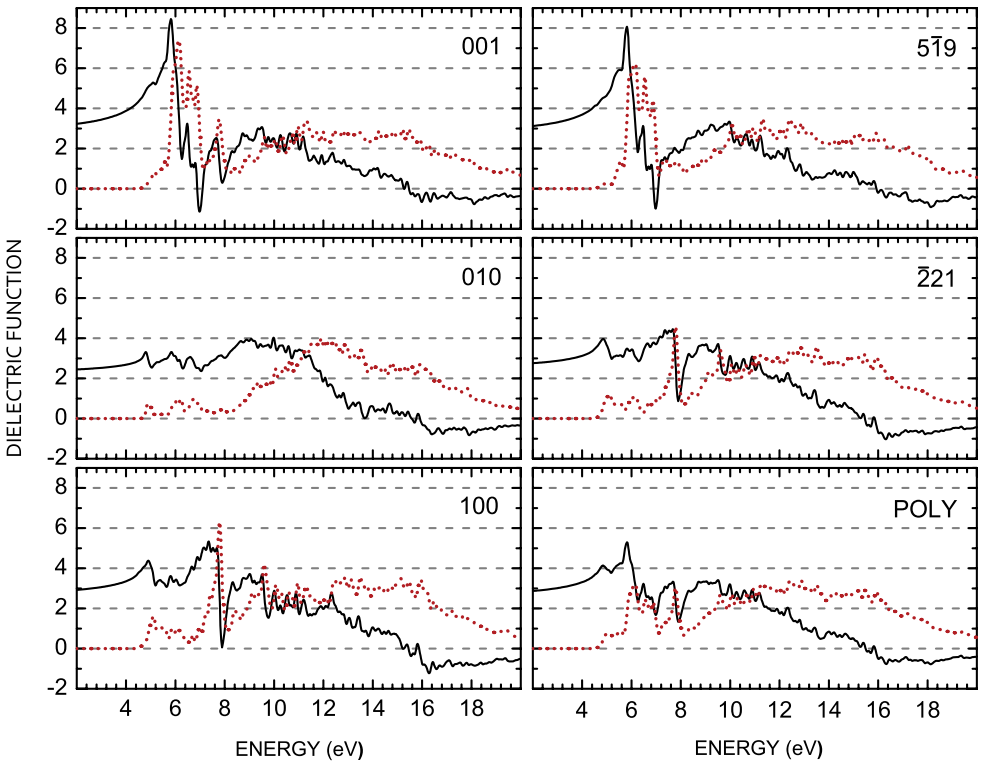

FIG. 13. (Color online) Real (solid line) and imaginary (dotted line) components of the LDA calculated dielectric function of the anhydrous aspartic acid crystal along the directions 001, 010, 100, 5$\bar{1}$9, and $\bar{2}$21. The dielectric function components for the polycrystal are also shown.

with experiment. The unit-cell total-energy dependence on the lattice parameters indicates that the crystal is softer along the *b* direction, which can be related to the weaker character of the hydrogen bonds between *L*-aspartic acid molecules in different molecular planes. Hirshfeld population analysis has shown that the most negatively charged atoms in an *L*-aspartic acid molecule embedded in the anhydrous crystal are O_1, O_2, and O_3, whereas the C_1 carbon atom is the most positively charged, giving us insight into the dipole strength of the zwitterionic state. The Kohn-Sham band structures, in contrast, have shown that *L*-aspartic acid anhydrous crystals have a set of close indirect band gaps, the smallest one being 4.49 eV ($B \rightarrow \alpha_1$), according with the GGA + D computation. This value is approximately 0.5 eV lower than the 5.02 eV estimate from our optical absorption measurements. In order to investigate the charge carrier transport features, we have also estimated the effective masses of electrons and holes, obtaining a very anisotropic behavior. For charge transport parallel to the molecular planes in the unit cell, the hole (electron) effective mass, obtained from the GGA + D corresponding band curve, is 1.46 (2.46) free-electron masses, whereas for transport along the perpendicular direction we have a hole (electron) effective mass of 11.68 (5.05) free-electron masses. We can conclude, therefore, that at least for an electric field applied parallel to the molecular planes of *L*-aspartic acid, the anhydrous *L*-aspartic acid crystals must behave as a wide-band-gap semiconductor, which could be interesting for bio-organic electronic and bionanoelectronic applications. Finally, the calculated complex dielectric function reveals a significant degree of optical anisotropy, with the real part of the dielectric function along the directions parallel and perpendicular to the *L*-aspartic acid molecular planes being very similar to the 001 and 100 curves independently from the exchange-correlation functional chosen.

ACKNOWLEDGMENTS

V.N.F. and E.L.A. would like to acknowledge financial support received during the development of this work from the Brazilian Research Agency Conselho Nacional de Desenvolvimento Científico e Tecnológico (CNPq). E.W.S.C. received financial support from CNPq Projects No. 304283/2010-0 and No. 474734/2011-0. This work was partially financed by the Brazilian Research Agencies Coordenação de Aperfeiçoamento de Pessoal de Nível Superior (PROCAD and Rede NanoBioTec), CNPq [INCT-Nano(Bio)Simes, Project No. 573925/2008-9], and Fundação para o Apoio de Pesquisa do Rio Grande do Norte CNPq (Pronex).

[1]T. Lee and Y. K. Lin, Cryst. Growth Des. **10**, 1652 (2010).
[2]R. H. A. Plimmer, *The Chemical Constitution of the Proteins* (Longmans, Green and Co., London, 1908).
[3]H. R. Stennike, Cell Death Differ. **6**, 1054 (1999).
[4]A. Cavallero, A. Marte, and E. Fedele, J. Neurochem. **110**, 924 (2009).
[5]M. C. Chen and Z. Lin, J. Chem. Phys. **127**, 154314 (2007).

[6]M. E. Sanz, J. C. López, and J. L. Açomso, Phys. Chem. Chem. Phys. **12**, 3573 (2010).
[7]C. Viedma, J. E. Ortiz, T. De Torres, T. Izumi, and D. G. Blackmond, J. Am. Chem. Soc. **130**, 15274 (2008).
[8]J. D. Bernal, Z. Kristallogr. **78**, 363 (1931).
[9]J. L. Derissen, H. J. Endeman, and A. F. Peerdeman, Acta Cryst. B **24**, 1349 (1968).
[10]K. Umadevi, K. Anitha, B. Sridhar, N. Srinivasan, and R. K. Rajaram, Acta Cryst. E **59**, o1073 (2003).
[11]S. T. Rao, R. Srinivasan, and V. Valambal, Indian J. Pure Appl. Phys. **6**, 523 (1968).
[12]S. T. Rao, Acta Crystallogr. Sect. B **29**, 1718 (1973).
[13]A. Sequeira, H. Rajagopal, and M. Ramanadham, Acta Crystallogr. Sect. C **45**, 906 (1989).
[14]G. W. Wang, L. Zeng-Xin, D. Chun-Sheng, and H. Li, Acta Crystallogr. Sect. E **63**, o4003 (2007).
[15]P. R. Tulip and S. J. Clark, Phys. Rev. B **71**, 195117 (2005).
[16]E. W. S. Caetano, J. R. Pinheiro, M. Zimmer, V. N. Freire, G. A. Farias, G. A. Bezerra, B. S. Cavada, J. R. L. Fernadez, J. R. Leite, M. C. F. de Oliveira, J. A. Pinheiro, J. L. de Lima Filho, and H. W. Leite Alves, in *Proceedings of the 27th International Conference on the Physics of Semiconductors*, edited by J. Menéndez and C. Van de Walle, AIP Conf. Proc. No. 772 (AIP, New York, 2005), p. 1095.
[17]M. Z. S. Flores, V. N. Freire, R. P. dos Santos, G. A. Farias, E. W. S. Caetano, M. C. F. de Oliveira, J. R. L. Fernandez, L. M. R. Scolfaro, M. J. B. Bezerra, T. M. Oliveira, G. A. Bezerra, B. S. Cavada, and H. W. Leite Alves, Phys. Rev. B **77**, 115104 (2008).
[18]R. L. Willett, K. W. Baldwin, K. W. West, and L. N. Pfeiffer, Proc. Natl. Acad. Sci. USA **102**, 7817 (2005).
[19]M. Oda and T. Nakayama, Jpn. J. Appl. Phys. 1 **45**, 8939 (2006).
[20]M. Oda and T. Nakayama, Appl. Surf. Sci. **244**, 627 (2005).
[21]M. A. Stroscio and M. Dutta, Proc. IEEE **93**, 1772 (2008).
[22]F. F. Maia Jr., V. N. Freire, E. W. S. Caetano, D. L. Azevedo, F. A. M. Sales, and E. L. Albuquerque, J. Chem. Phys. **134**, 175101 (2011).
[23]J. R. Cândido-Júnior, F. A. M. Sales, S. N. Costa, P. De Lima-Neto, D. L. Azevedo, and E. W. S. Caetano, Chem. Phys. Lett. **512**, 208 (2011).
[24]M. Irimia-Vladu, N. S. Sariciftci, and S. Bauer, J. Mater. Chem. **21**, 1350 (2011).
[25]V. Parpura, Nat. Nanotechnol. **7**, 143 (2012).
[26]H. Y. Fan, Rep. Prog. Phys. **19**, 107 (1956).
[27]A. M. Fox, in *Optical Properties of Solids* (Oxford University Press, Oxford, 2001), p. 58.
[28]D. Segall, P. J. D. Lindan, M. J. Probert, C. J. Pickard, P. J. Hasnip, S. J. Clark, and M. C. Payne, J. Phys.: Condens. Matter **14**, 2717 (2002).
[29]S. K. Medeiros, E. L. Albuquerque, F. F. Maia Jr., E. W. S. Caetano, and V. N. Freire, Chem. Phys. Lett. **435**, 59 (2007).
[30]R. Demichelis, P. Raiteri, J. D. Gale, and R. Dovesi, CrystEngComm **14**, 44 (2012).
[31]P. Hohenberg and W. Kohn, Phys. Rev. B **136**, 864 (1964).
[32]W. Kohn and L. J. Sham, Phys. Rev. **140**, A1133 (1965).
[33]D. M. Ceperley and B. J. Alder, Phys. Rev. Lett. **45**, 566 (1980).
[34]J. P. Perdew and A. Zunger, Phys. Rev. B **23**, 5048 (1981).
[35]J. P. Perdew, K. Burke, and M. Ernzerhof, Phys. Rev. Lett. **77**, 3865 (1996).
[36]A. Tkatchenko and M. Scheffler, Phys. Rev. Lett. **102**, 073005 (2009).
[37]J. P. Perdew and Y. Wang, Phys. Rev. B **45**, 13244 (1992).
[38]J. S. Lin, A. Qteish, M. C. Payne, and V. Heine, Phys. Rev. B **47**, 4174 (1993).
[39]H. J. Monkhorst and J. D. Pack, Phys. Rev. B **13**, 5188 (1976).
[40]B. G. Pfrommer, M. Cote, S. G. Louie, and M. L. Cohen, J. Comput. Phys. **131**, 133 (1997).
[41]See Supplemental Material at http://link.aps.org/supplemental/10.1103/PhysRevB.86.195201 for results of the GGA + D and LDA calculations.
[42]R. S. Mulliken, J. Chem. Phys. **23**, 1833 (1955).
[43]F. L. Hirshfeld, Theor. Chim. Acta **44**, 129 (1977).
[44]R. K. Roy, K. Hirao, S. Krishnamurty, and S. Pal, J. Chem. Phys. **115**, 2901 (2001).
[45]R. K. Roy, S. Pal, and K. Hirao, J. Chem. Phys. **110**, 8236 (1999).
[46]R. G. Parr and W. T. Yang, J. Am. Chem. Soc. **106**, 4049 (1984).
[47]J. P. Foster and F. Weinhold, J. Am. Chem. Soc. **102**, 7211 (1980).
[48]R. Bonaccorsi, E. Scrocco, and J. Tomasi, J. Chem. Phys. **52**, 5270 (1970).
[49]P. W. Ayers, R. C. Morrison, and R. K. Roy, J. Chem. Phys. **116**, 8731 (2002).
[50]R. F. Nalewajski and R. G. Parr, Proc. Nat. Acad. Sci. USA **97**, 8879 (2000).
[51]E. R. Davidson and S. Chakravorty, Theor. Chim. Acta **83**, 319 (1992).
[52]P. Bultinck, C. Van Alsenoy, P. W. Ayers, and R. Carbó-Dorca, J. Chem. Phys. **126**, 144111 (2007).
[53]P. W. Ayers, Theor. Chem. Acc. **115**, 370 (2006).
[54]R. G. Parr, P. W. Ayers, and R. F. Nalejawski, J. Phys. Chem. A **109**, 3957 (2005).
[55]T. Verstraelen, S. V. Sukhomlinov, V. Van Speybroeck, M. Waroquier, and K. S. Smirnov, J. Phys. Chem. C **116**, 490 (2012).
[56]P. Bultinck, S. Fias, C. V. Alsenoy, P. W. Ayers, and R. Carbó-Dorca, J. Chem. Phys. **127**, 034102 (2007).
[57]A. Seidl, A. Gorling, P. Vogl, J. A. Majewski, and M. Levy, Phys. Rev. B **53**, 3764 (1996).
[58]J. P. Perdew and M. Levy, Phys. Rev. Lett. **51**, 1884 (1983).
[59]L. J. Sham and M. Schluter, Phys. Rev. B **32**, 3883 (1985).
[60]L. J. Sham and M. Schluter, Phys. Rev. Lett. **51**, 1888 (1983).
[61]A. J. Cohen, P. Mori-Sanchez, and W. T. Yang, Phys. Rev. B **77**, 115123 (2008).
[62]X. Zheng, A. J. Cohen, P. Mori-Sanchez, X. Q. Hu, and W. T. Yang, Phys. Rev. Lett. **107**, 026403 (2011).
[63]A. Klamt and G. Schüürmann, J. Chem. Soc., Perkin Trans. **2**, 799 (1993).
[64]B. Delley, J. Chem. Phys. **113**, 7756 (2000).